Journal of Applied Polymer Science

Binder-free porous PEDOT electrodes for flexible supercapacitors

Qiang Zhao,[1] Guixin Wang,[1] Kangping Yan,[1] Jixin Yan,[2] Jianzhong Wang[2]
[1]College of Chemical Engineering, Sichuan University, Chengdu 610065, China
[2]Postdoctoral Scientific Research Workstation, Jiangsu United Technology Group, Tongzhou 226361, China
Correspondence to: G.X. Wang (E-mail: guixin66@scu.edu.cn) and K.P. Yan (E-mail: yankp@scu.edu.cn)

ABSTRACT: Conducting polymers are attractive for potential applications in flexible electronic industries because of their unique advantages. To simplify the process of electrode preparation, porous poly(3,4-ethylenedioxythiophene) (PEDOT) film electrodes without binder and conductive additive were synthesized facilely for flexible supercapacitors via an *in situ* solution micro polymerization at the surface of a soft etched tunnel aluminum (ETA) template at room temperature. The template was directly used as the current collector of electrodes. The morphologies of the samples and the template were compared using scanning electron microscopy (SEM), and the polymer molecular structure and composition were analyzed with Fourier-transform infrared (FTIR) spectroscopy. Symmetric supercapacitors were assembled with the PEDOT electrodes, Celgard 2300 separator, and 1.0 *M* $LiPF_6$/EC+DMC+EMC (1 : 1 : 1 in volume) electrolyte. The electrochemical performance was evaluated using different techniques like galvanostatic charging/discharging tests, cyclic voltammetry (CV), and electrochemical impedance spectroscopy (EIS). The results from different current densities and scanning rates show the supercapacitors have good rate performance. The specific capacitance, energy density, and coulombic efficiency of the PEDOT supercapacitor can reach 69.0 F g^{-1} (or 103.0 F m^{-2}), 24.0 Wh kg^{-1}, and ~95% at a current density of 0.2 A g^{-1}, respectively. Furthermore, the PEDOT electrodes exhibit relatively good cycle performance, and the capacitance retention ratio is ~72% after 1500 cycles. The electrode process was discussed. The results are comparable to that of the reported PEDOT, which indicates the applicability of the novel simple method of solution microreaction at the surface of a soft metal template to directly prepare binder-free flexible electrodes. © 2015 Wiley Periodicals, Inc. J. Appl. Polym. Sci. **2015**, *132*, 42549.

KEYWORDS: conducting polymers; electrochemistry; films; surfaces and interfaces

Received 26 December 2014; accepted 25 May 2015
DOI: 10.1002/app.42549

INTRODUCTION

With the rapid development of portable flexible electronic devices with miniaturization and wearability,[1] novel flexible energy storage technologies have gained increasing attention and will become a field with tremendous opportunities.[2,3] As one of the attractive power sources, supercapacitors are highly anticipated to satisfy the demands of such flexible devices.[4] Supercapacitors, also known as ultracapacitors or electrochemical capacitors, integrate the advantages of batteries and conventional capacitors, which makes them very promising for high-power and high-energy applications like (hybrid) electric vehicles, regenerative braking, burst-mode power delivery, or portable electronics. According to different energy storage mechanisms, supercapacitors can be categorized into electric double-layer capacitors (EDLC) and pseudocapacitors.[5] The former stores energy by physically separating positive and negative electric charges in the Helmholtz layer at the interface between an electrode and an electrolyte, and the latter is based on fast and reversible Faradaic electron charge-transfer with redox reactions, intercalation or electrosorption. To simultaneously utilize the high power of EDLC and the high energy of pseudocapacitors, hybrid capacitors (also called asymmetric capacitors, such as capbatteries composed of battery electrode materials and carbons), have been developed by combining the above two energy storage mechanisms using an electrochemical cathode and an electrostatic anode. In fact, the capacitance of a supercapacitor is composed of both electric double-layer capacitance and pseudocapacitance, where one is usually dominant. Due to the similar energy storage mechanism to batteries, pseudocapacitance is generally higher than electric double-layer capacitance under the same conditions. Therefore, many redox energy materials, such as MnO_y,[6,7] NiO_y,[8] $LiFePO_4$,[9] $LiMn_2O_4$,[10] $LiNi_{0.8}Co_{0.2}O_2$,[11] $Li_4Ti_5O_{12}$,[12] PEDOT,[13–16] polypyrrole (PPy),[17] and polyaniline (PAN),[18] have been used to improve the capacitance of current supercapacitors.

To develop flexible supercapacitors, plenty of ductile materials, including porous carbons (mesoporous carbon,[7,19] graphene,[20] and carbon nanotubes[21]), traditional capacitive materials,[22,23]

and polymers,[24] have been investigated. Electronically conducting polymers (ECPs) are promising to prepare flexible electrodes owing to their advantages such as high plasticity and thermal stability, fast doping/undoping process, different doping levels, a wide range of electric conductivity, and plentiful of raw materials.[25] However, the poor cycling stability of such ECPs, mainly from volumetric changes (swelling, shrinking, cracks or breaking) during ion insertion/extraction process,[14,26] prevents their extensive applications. Therefore, specific morphology and good electric contact to current collector are crucial to ensure active materials to be fully utilized[27] and to alleviate the volumetric changes to retard the capacitance fade and the aggravation of conducting properties. One way to achieve this goal is to add conductive additive to the electrodes for better electric conductivity, but it makes the preparation process very complex because of the difficult dispersion. Another way is to control morphology like nanoparticles,[28,29] or nanotubes,[30,31] which leads to a short pathway for good charge transport and electric contact between active materials and current collector.[32] On the other hand, binders, such as polyvinylidene fluoride (PVDF), polytetrafluoroethene (PTFE), carboxymethyl cellulose (CMC), and styrene-butadiene rubber (SBR), are always used to paste active materials to current collector in conventional electrodes, but they stand in the way of improving the electrochemical performance of electrodes with poor conductivity, increasing cost and simplifying preparation process.

As one of the important π-conjugated ECPs, PEDOT has attracted growing interests in the field of functional materials because of its available electronic conductivity, fast charge/discharge kinetics[33] and good environmental compatibility.[34] Different PEDOT electrodes have been explored for supercapacitors.[13–16] However, the molecular structure makes it difficult for PEDOT to form thin films, fibrils, or tubes.[16,30,35,36] Thus, *in situ* polymerization, including ZnO arrays[37] and anodic alumina oxide (AAO) templates,[30,35] is widely used in the formation of PEDOT with special morphology. In comparison to AAO template, etched tunnel aluminum (ETA) template has many advantages such as good strength and toughness, high conductivity of about 3.6×10^7 S m^{-1}, large pore size, and high thickness, so such template does not need to be removed and can be continuously used as the current collector of electrodes, which is different from ordinary way to remove the template after the formation of product. We have easily synthesized highly ordered PEDOT tube arrays with hierarchical structure and high aspect ratio by an *in situ* high-gravity reaction polymerization using ETA templates.[27] Microreaction technology has moved into the mainstream of current synthesis industries because of the advantages like good transfer properties, short diffusion distances, and safety.[38] Porous ETA templates can be used as both the micro reactor for the synthesis of PEDOT film and the current collector of flexible electrodes. Considering the wide electrochemical window that is closely related to energy density and power density, an organic electrolyte was chosen.

Herein, a novel facile method was developed to prepare flexible film electrodes. PEDOT film electrodes without binder and conductive additive have been easily prepared by an *in situ* solution micro polymerization at the surface of ETA soft metal templates at room temperature. After being tailored, the ETA templates coated with polymer film were utilized to construct flexible supercapacitors with an organic electrolyte. The electrochemical performance of the supercapacitors was investigated by different techniques, and the possible reaction mechanism was discussed.

EXPERIMENTAL

High-purity aluminum foils (99.999 wt %, ~110 μm in thickness, provided by Jiangsu United Technology Group, China) were used to prepare ETA templates by the method of galvanostatic electrochemical etching.[27,39] After being heated in air, the aluminum foils were etched in a mixed acid of H_2SO_4 and HCl (3 : 1 in mol) at ~80°C with a current density of 0.2 A cm^{-2} in a two-electrode compartment with a high purity graphite counter electrode. After being rinsed with high-purity deionized water (specific resistance of ~18 MΩ cm) repeatedly, the ETA templates were dried for later use. Besides a large area of more than 0.5 m×1.0 m, such templates can be arbitrarily rolled.

PEDOT film electrodes were prepared by an *in situ* chemical micro polymerization of precursor solution film at the surface of the porous ETA templates, and the synthesis scheme is supplied in Figure 1. Firstly, about 6 μL reducing agent of 3,4-ethylenedioxythiophene (EDOT) monomer (~99 wt %) was added to the surface of the as-synthesized ETA template using a micro-syringe and kept at room temperature for 10 min to allow the solution fully wet the template to form a thin film via infiltration, [Figure 1(C)]. Secondly, about 44 μL n-butanol solution of Fe(III) p-toluene-sulfonate oxidant (FeTos, ~55 wt %) was added to the above template surface covered with EDOT monomer, and then the ETA template with EDOT and FeTos solution film was kept at room temperature for 2 h to complete the reaction [Figure 1(D,E)]. Capillary attraction draws EDOT and FeTos solutions into, around, and all about the pores of ETA template, so PEDOT was obtained at the surface of the template. One side of the PEDOT coated template was polished for its better contact with current collector from capacitor setup. After being washed repeatedly with ethanol and deionized water to remove the impurities and unreacted raw materials, the ETA template covered with sample film was dried overnight in an oven at 70°C in air, and then was cut into slice to use as electrodes. The weight of the active material was calculated by the mass difference of the electrode before and after being calcined at 500°C in air via the contrast experiments to confirm that the mass of such ETA template is constant. The loading mass density of the active material on the macrographic surface area of the electrode is ~0.15 mg cm^{-2}.

The morphologies of the ETA templates and the PEDOT electrodes were observed using a field emission scanning electron microscopy (FESEM, FEI INSPECT F). The molecular structure and composition of the as-synthesized PEDOT material were characterized by a Fourier Transform Infrared Spectroscopy (FTIR) spectrum, which was carried out on a Thermo Nicolet Avatar 370 FTIR spectrometer. 1.0 *M* $LiPF_6$/EC+DMC+EMC (1 : 1 : 1 in volume) electrolyte and Celgard 2300 microporous separator were utilized, respectively. Symmetric supercapacitors (p/p) were assembled by sandwiching a separator impregnated

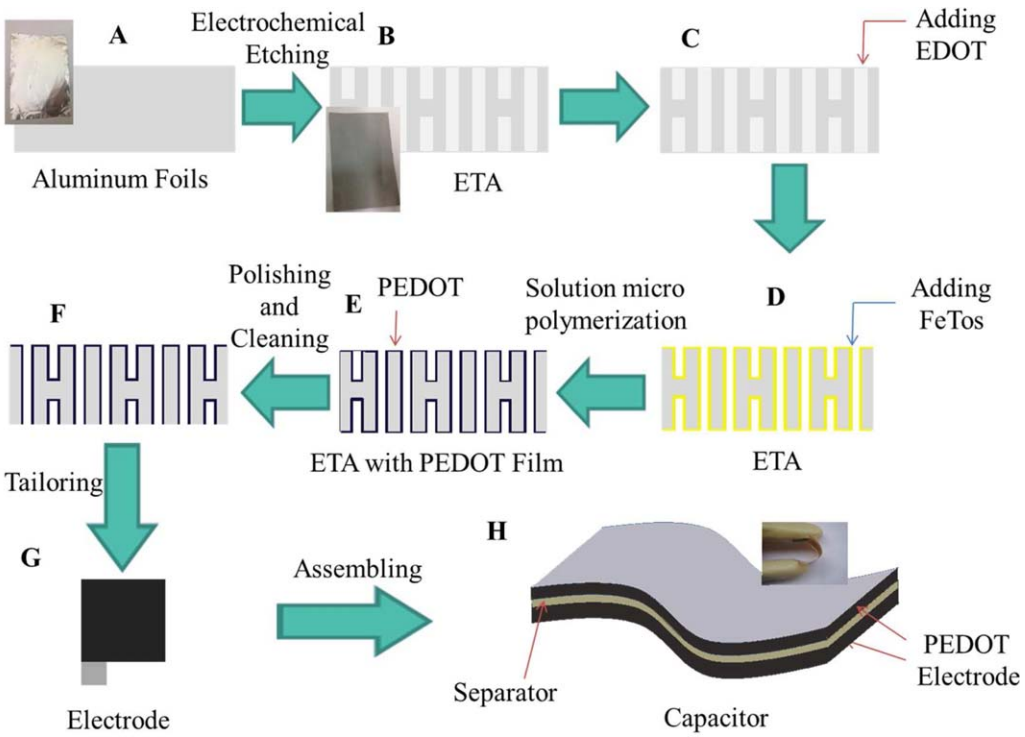

Figure 1. Schematic illustration of the fabrication of binder-free flexible PEDOT supercapacitors. (A,B) preparation of ETA templates, (C–F) preparation of PEDOT electrodes, and (G,H) assembly of PEDOT electrodes to fabricate supercapacitors. Inset in A, B, and H show optical images of aluminium foil, ETA template, and flexible capacitor, respectively. [Color figure can be viewed in the online issue, which is available at wileyonlinelibrary.com.]

with the electrolyte between two PEDOT electrodes which were pre-wetted with the electrolyte. The electrochemical performance was evaluated by different techniques such as cyclic voltammetry (CV), electrochemical impedance spectroscopy (EIS) in the frequency range of 100 kHz∼10 mHz, and galvanostatic charge/discharge cycling at difference current densities. The CV and EIS measurements were carried out on an electrochemical workstation which consists of a PAR 273A potentiostat/galvanostat and a signal recovery model 5210 lock-in-amplifier controlled by a Powersuit software (Princeton Applied Research, USA). The galvanostatic charge/discharge cycling was conducted on a Neware battery-testing instrument (Shenzhen Neware Technology, China).

RESULTS AND DISCUSSION

The scanning electron microscopy (SEM) images of the surface of the pristine and the product covered ETA templates are supplied in Figure 2. From the Figure 2(a,b), the pristine ETA template has a smooth surface and clear porous morphology. Large amounts of tunnels are vertical to the aluminum surface, and these tunnels are parallel and have a length of 40∼45 μm according to our previous research.[27] The transverse shape of the tunnels is quasi-square, and the tunnel pore density is estimated to be $\sim 10^7$ cm^{-2}. Some small pores connect together to form big ones, and the pore size ranges from 0.3 to 2 μm. After adding the yellow FeTos oxidant to the colorless EDOT reducer at the surface of the template, the silvery grey metallic luster of the pristine ETA template changes gradually to dark blue, indicating that the surface of the template is covered with a layer of the produced sample which has the same color with n-doped PEDOT polymer.[27,28,40] The film thickness, which can be well adjusted by controlling the reactant concentration and reaction time, is about 100 μm. Thus, most of the surface pores cannot be detected clearly, as shown in Figure 2(c,d). The porous ETA template is used as a microreactor, and the microscale raw materials of EDOT monomer and FeTos oxidant infiltrate to the porous surface of the template via capillary attraction, so a thin film of precursor solution will adsorb the surface and rapidly mix and react at the surface to produce a polymer film to cover the surface of the template. As a result, the PEDOT film is obtained successfully by an *in situ* solution micro polymerization at the porous surface of ETA template, which will be confirmed by the FTIR later. The large reaction surface and the microscale solution film make the reaction easily take place at room temperature in a short time. On the other hand, the ETA template has a high electric conductivity (similar to that of general aluminum current collector) because it is porous aluminum with a high purity, so the ETA template can be directly used as the current collector to prepare flexible electrodes without any binders. Furthermore, the porous structure of the current collector is beneficial for the formation of porous electrodes besides the wedging function to prevent electrode materials from falling off during cycles. Consequently, porous ETA template plays an important role in the formation of binder-free film electrodes because it is used as both the microreactor for film formation and the current collectors of electrodes.

In order to determine the chemical structure and composition of the sample on the ETA template, FTIR analysis was

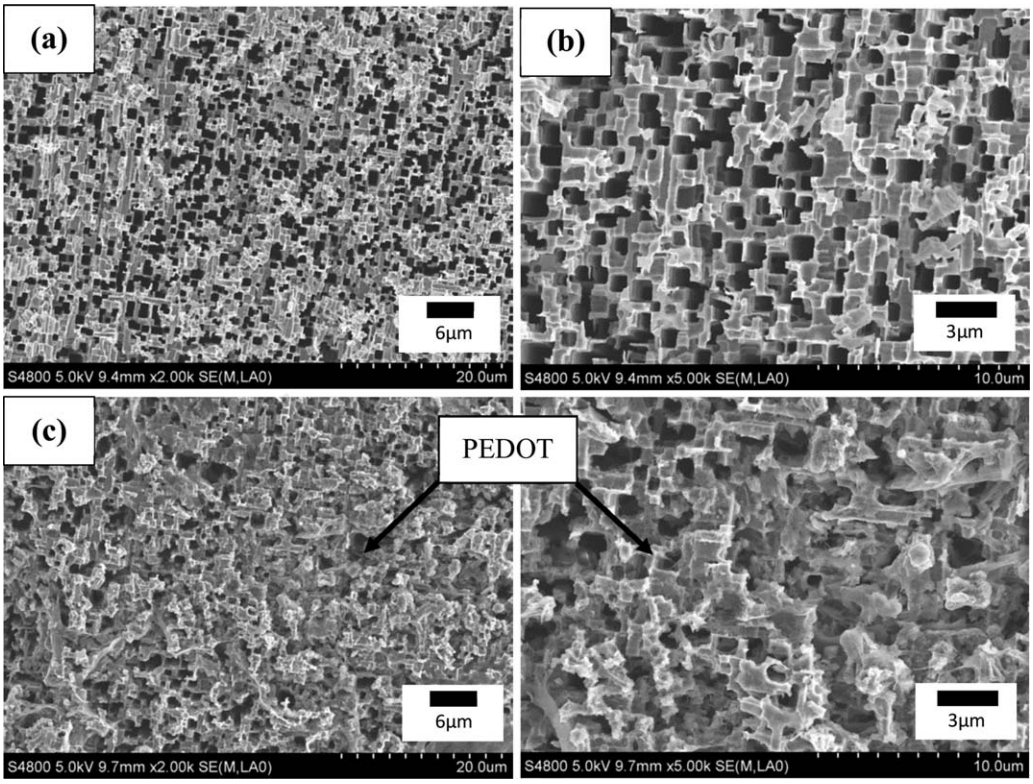

Figure 2. FESEM images of the pristine (a,b), and sample coated ETA templates (c,d).

conducted by removing the ETA template using a 0.5 *M* NaOH solution,[27] and the result is shown in Figure 3. The vibrational bands at 1541∼1421 cm^{-1} and 1393∼1336 cm^{-1} are due to $C_\alpha{=}C_\beta$ asymmetric stretching and $C_\alpha{-}C_\beta$ stretching, respectively.[27–28] The peaks at 1194∼852 cm^{-1} are associated with the stretching of the alkylenedioxy group.[29] The absorption at ∼1645 cm^{-1} is assigned to the doped level of PEDOT,[27,29] consistent with the dark blue color of the sample.[30–32] The bands at 1421∼1194 cm^{-1} are referred to the stretching of the sulfonic group.[30,33] These results demonstrate that the product is PEDOT, indicating the surface of the ETA template is covered with PEDOT polymer film.

To evaluate the electrochemical performance, two-electrode supercapacitors with symmetric structure were assembled by using above PEDOT electrodes. From the cyclic voltammetry (CV) curves of the PEDOT supercapacitor in Figure 4, the curves have a quasi-rectangle shape, no obvious redox peaks, indicating the as-synthesized PEDOT shows a typical ideal capacitive feature.[5] Furthermore, the current response increases with the increase of scanning rate, while the CV curves keep the ideal quasi-rectangular shape when the scanning rate increases from 1 to 10 mV s^{-1}, indicating the rate performance of the as-synthesized polymer is good, which will be further demonstrated by the following constant current testing results.

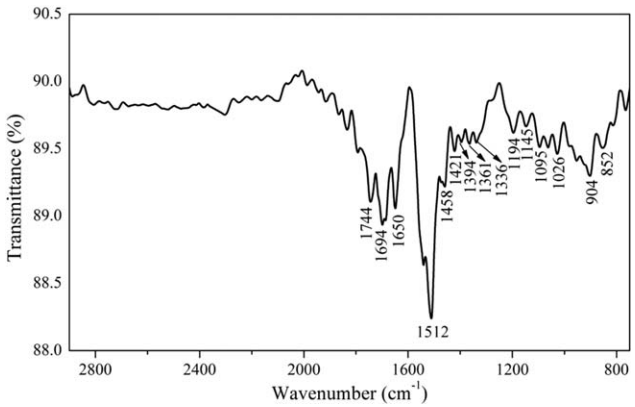

Figure 3. FTIR spectrum of the as-synthesized sample.

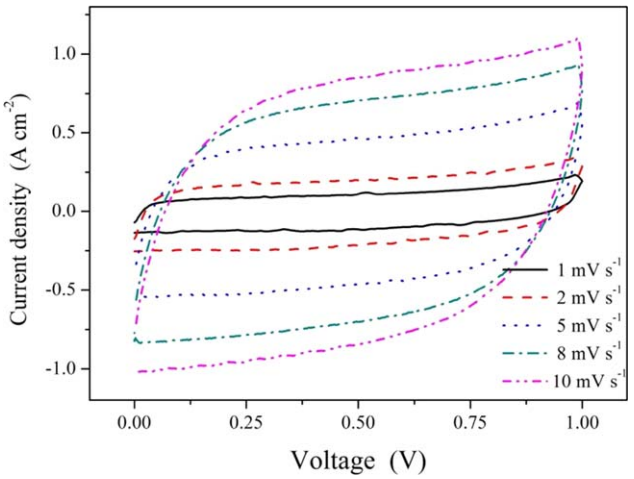

Figure 4. Cyclic voltammetry curves of the PEDOT supercapacitor with different scanning rates. [Color figure can be viewed in the online issue, which is available at wileyonlinelibrary.com.]

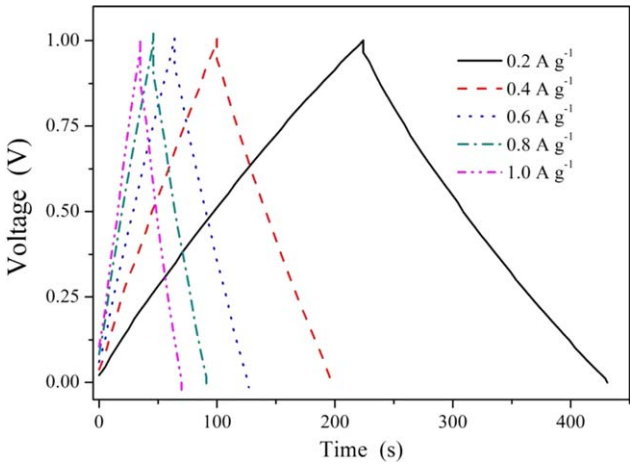

Figure 5. Galvanostatic charge/discharge curves of the PEDOT supercapacitor at different current densities. [Color figure can be viewed in the online issue, which is available at wileyonlinelibrary.com.]

The representative galvanostatic charge/discharge curves of the PEDOT supercapacitor are summarized in Figure 5. To obtain the stable values under different current densities, the tenth charge/discharge cycles were chosen for electrochemical analysis if not specified. Except the small part of the iR (combined effects of current and resistance) drop of the supercapacitor at the joint between the charging end and the discharging start, the potential is linear with the corresponding time, and the charging/discharging curves are almost symmetric, indicating the material has a good supercapacitive property. With the current density increasing from 0.2 to 1.0 A g^{-1}, the linear relationship changes little, indicative of good rate performance. These results agree well with that of above CV tests. However, the iR drop increases with the increase of current density, indicating the polarization resistance increases. From the linear part of the discharging curves, the values of the total specific capacitance (C_t) of the supercapacitor can be calculated according to the following formula.

$$C_t = \frac{I \cdot dt}{m_t \cdot dU} \tag{1}$$

where I (A), m_t (g), dU (V), and dt (s) are the applied current, the total mass of the active materials in both positive and negative electrodes, the voltage change, and the corresponding time change of the capacitor during the discharging process, respectively. In a symmetric capacitor, two equivalent electrodes are connected in series, so the capacitance of one electrode is twice that of the total capacitance according to the principle of a plate capacitor.[34] Therefore, the values of the mass specific capacitance (C_m) and the area specific capacitance (C_a) of the active material can be calculated according to the following equations.

$$C_m = 2\times\frac{I \cdot dt}{m \cdot dU} = 4\times\frac{I \cdot dt}{m_t \cdot dU} \tag{2}$$

$$C_a = 2\times\frac{I \cdot dt}{a \cdot dU} \tag{3}$$

where m(g) is the mass of the active material in one electrode, which is half of the m_t because of the consistent positive electrode and negative electrode without considering other compositions, and a (m^{-2}) is the macrographic surface area of one electrode disc.

Columbic efficiency η can be calculated by the following formula

$$\eta = \frac{C_d}{C_c} \tag{4}$$

where C_d and C_c are the discharge capacitance and the charge capacitance, respectively.

Energy density E (Wh kg^{-1}) and power density P (W kg^{-1}) of the capacitor, can be calculated according to the following equations.

$$E = 3.6\times\frac{I\int_0^t U dt}{m_t} = 1.8 \times C_t U^2 \tag{5}$$

$$P = \frac{1}{1000}\times\frac{I \cdot U}{m_t} = \frac{E}{t'} \tag{6}$$

where U and t' are the discharge voltage and the corresponding time in hour of a capacitor, respectively.

According to the typical linear discharge curves, the experimental values of C_m, C_a, E, P, and η were obtained by using above equations. The influence of current density on the capacitance, energy density, and coulombic efficiency as well as the Ragone plot is provided in Figure 6. From Figure 6(a,b), the mass specific capacitance and the area specific capacitance of the PEDOT supercapacitor after ten cycles are 69.0 F g^{-1} and 103.0 F m^{-2} at the current density of 0.2 A g^{-1}, and they decrease to 58.3 F g^{-1} and 87.5 F m^{-2} when the current density reaches 1.0 A g^{-1}, respectively. Based on above capacitance relationship between electrode and capacitor, the mass specific capacitance and the area specific capacitance of the PEDOT electrode are 276.0 F g^{-1} and 206.0 F m^{-2} at 0.2 A g^{-1}, while they are 233.2 F g^{-1} and 175.0 F m^{-2} at 1.0 A g^{-1}, respectively. These values are higher than that of the reported PEDOT[13,32–35] and other conducting polymers like PPy[17] under the similar testing conditions. From Figure 6(c), the coulombic efficiency increases from ~92% to ~100% when the current density increases from 0.2 to 1.0 A g^{-1}, indicative of a good reaction reversibility except the initial activation process. From Figure 6(d,e), the energy density of the PEDOT supercapacitor decreases from ~24.0 to ~20.3 Wh kg^{-1} when the corresponding power density increases from ~420 to ~2080 W kg^{-1}, and the energy retention ratio is about ~85% when the current density increases from 0.2 to 1.0 A g^{-1}. Noticeably, the energy density and the power density of the PEDOT supercapacitor are also higher than that of the reported ones based on PEDOT powders[13] and other conducting polymers like PPy.[17] Furthermore, the PEDOT supercapacitor has a relatively good cyclability and high reaction reversibility, as shown in Figure 7. After 1500 cycles at the current density of 0.8 A g^{-1}, the retained capacitance is still ~72% of the initial value, while the coulombic efficiency remains above 95% during the cycles except the initial ~90%, much higher than that of the reported polymer supercapacitors using PEDOT powders,[13,36] PAN,[18,37] and PPy.[36] The low initial coulombic efficiency is from the electrode activation reaction at the beginning of the cycles.

The increased performance, including capacitance, energy density, cyclability, and coulombic efficiency, is from the special morphology and texture of the PEDOT electrodes. The unique

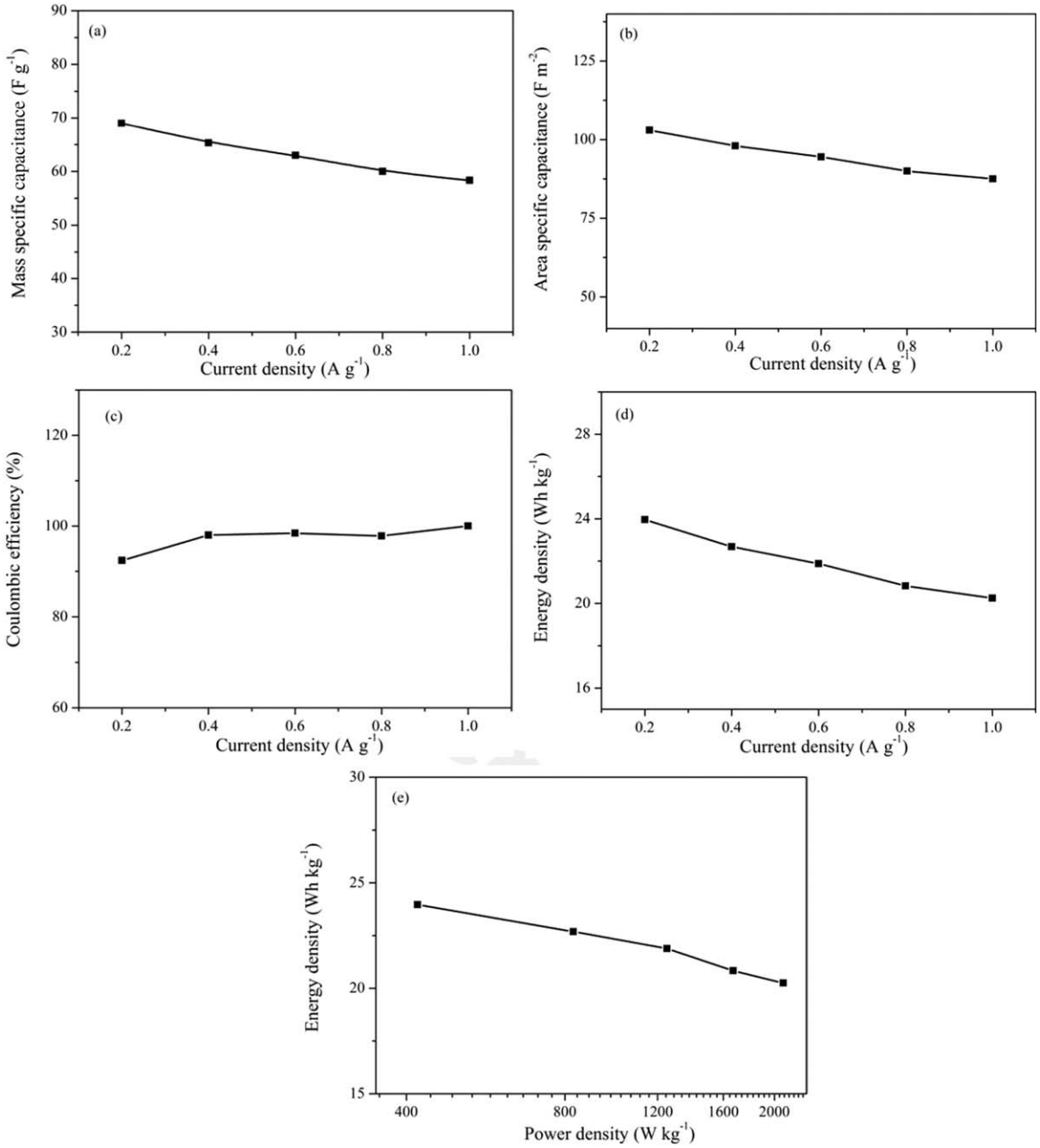

Figure 6. Mass specific capacitance (a), area specific capacitance (b), coulombic efficiency (c), and energy density (d) at various current densities, and Ragone plot (e) of the PEDOT supercapacitor.

porous structure of the PEDOT film have many obvious advantages, such as the storage of electrolytes and intermediate products, the high accessible surface area, the large interface between the active materials and the electrolyte, the increased microreaction active sites, the close contact between the active material and the current collector, the alleviated volume swelling and shrinking of the polymer during the charging/discharging process, and so on. At the same time, the slight capacitance fade may be from the degradation of PEDOT and the consumption of the electrolyte upon oxidation/reduction reactions.[40] As a whole, the as-synthesized binder-free porous PEDOT film electrodes are attractive candidates for energy storage with high efficiency.

In order to investigate the reaction mechanism of the PEDOT electrodes, EIS was conducted on the fresh PEDOT supercapacitor at an open circuit voltage of ~0.0 V, and the Nyquist plot is presented in Figure 8(a). There is a small semicircle in the high-middle frequency region and almost a straight line in the low frequency region. The straight line part leans more towards imaginary axis, indicative of a good capacitive behavior.[13,17] The intercept of the curve on the Z' axis in the high-frequency region is concerned on the Ohmic resistance of the electrolyte, while the depressed semicircle is associated with the electrode resistance, electrolyte film, and charge transfer impedances. The oblique line in low frequency region corresponds to Warburg impedance and bulk capacitance. The EIS curves are fitted using

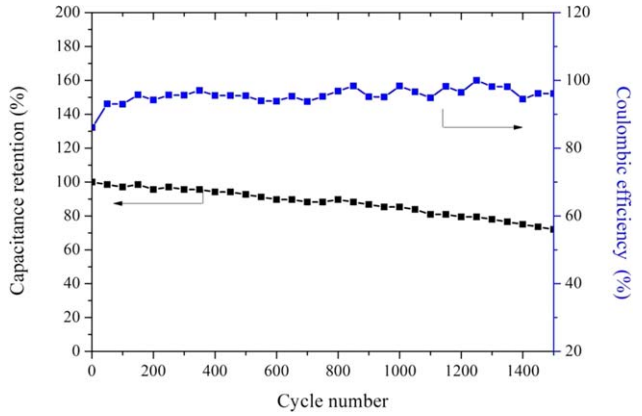

Figure 7. Cycling performance of the as-synthesized flexible PEDOT supercapacitor at the current density of 0.8 A g^{-1}. [Color figure can be viewed in the online issue, which is available at wileyonlinelibrary.com.]

the equivalent circuit model of $R_s(Q_l(R_i(Q_2R_f)(Q_3(R_{ct}W))))C_d$ in Figure 8(b), and the average error χ^2 is about 9.37×10^{-4}, indicative of the goodness of the above equivalent circuit model fitting of the tested EIS curve. Considering the nonhomogeneity such as porosity, roughness, and geometry in the system, constant phase element (CPE) Q is used to substitute for capacitance C.[39] Q is defined as $Z_{CPE} = [T(j\omega)^P]^{-1}$ according to the non-ideal capacitive behavior of the interface and the influence of the frequency dispersion phenomena,[40] where T and P are frequency independent parameters related to temperature, and $-1 \leq P \leq 1$. Q corresponds to an ideal capacitor when $P = 1$, an ideal resistor when $P = 0$, and a Warburg component when $P = 0.5$.[41] When a CPE is placed in parallel to a resistor, a depressed semicircle (core-element) will appear, as shown in Figure 8(a). In the equivalent circuit, R_s is the solution resistance.[42] Q_1 is the constant phase element (CPE) of the interface between electrode and electrolyte. R_i is the interface resistance between electrode and electrolyte film and its parameter values calculated by Zsimpwin is 3.21 Ω·cm^2. R_f refers to the resistance of the electrolyte film on the electrode, and Q_2 is the corresponding constant phase element (CPE). R_{ct} and W are the charge transfer reaction resistance and the Warburg impedance commonly representing the semi-infinite diffusion, respectively, and Q_3 is the corresponding constant phase element (CPE) of the reaction and diffusion interface. C_d refers to the bulk capacitance of the PEDOT electrode[43] and its fitting value from above equivalent circuit simulation is 4.73E-3 F cm^{-2}. The impedances connect the capacitance in series, indicating the bulk capacitance is much more important than the electric double-layer capacitance in the circuit, which shows that energy storage of the PEDOT electrode is based on the fast faradic redox reaction. Therefore, the PEDOT electrode capacitance is mainly from the Faradic pesudocapacitance.

According to the bode plot, the specific capacitance of a supercapacitor can be calculated by the following formula.

$$C_m = -\frac{1}{2 \times m \times \pi \times f \times Z''} \quad (7)$$

where C_m (F/g) is the mass specific capacitance, m (g) is the effective mass of activated materials, f (Hz) and $Z''(\Omega)$ are the

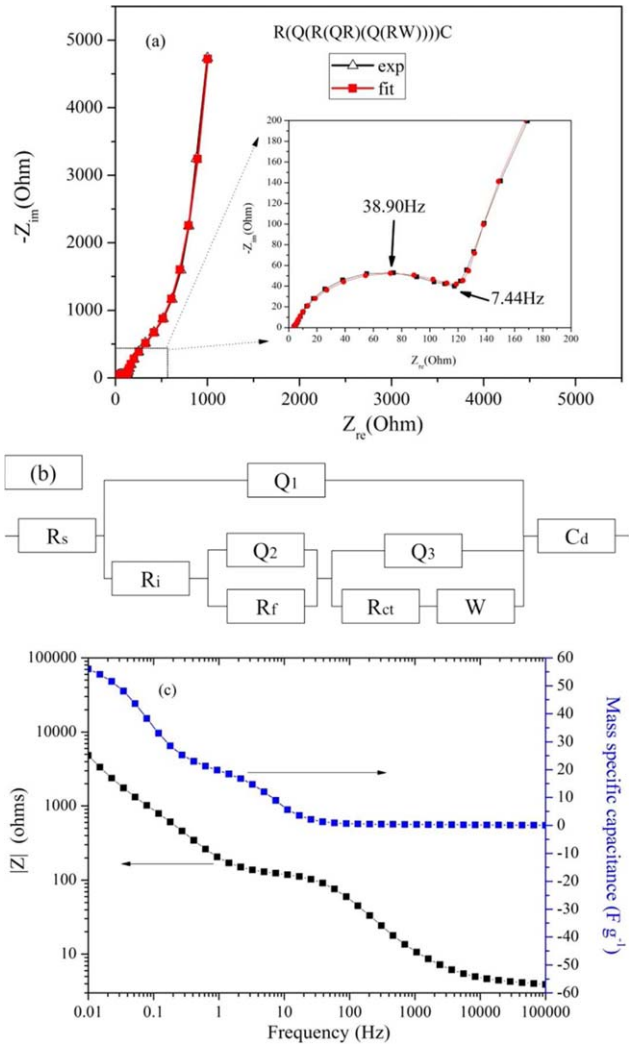

Figure 8. (a) Nyquist plot of the fresh PEDOT supercapacitor, inset is the magnified view of the plot at high-medium frequencies, (b) corresponding equivalent circuit model, and (c) Bode plot and calculated specific capacitance from EIS. [Color figure can be viewed in the online issue, which is available at wileyonlinelibrary.com.]

operating frequency and the corresponding imaginary component in an impedance plot, respectively. The influence of frequency on the capacitance is summarized in Figure 8(c). The capacitance value at low frequency is consistent with above galvanostatic charging/discharging results. When the frequency increases from 0.01 Hz to 20 Hz, the capacitance decreases quickly, but the capacitance remains almost zero when the frequency ranges from 20 Hz to 100 kHz.

The charge storage mechanism of PEDOT is shown in Scheme 1, and it mainly faradaically stores energy using the pseudocapacitance behavior of fast doping/undoping process.[44] When the frequency increases from 10 mHz to 20 Hz, the reaction time is shortened gradually from 100 s to 0.05 s, while the capacitance fades fast from 56.0 to 2.8 F g^{-1}, indicating the doping/undoping reaction process cannot complete in a short time. With the further increase of frequency from 20 Hz to 100 kHz, the capacitance is close to 0, indicating the electrode reaction almost

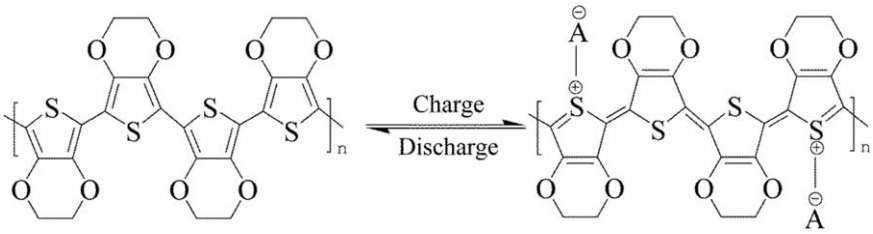

Scheme 1. Molecular structures of the oxidized and reduced forms of PEDOT (A^- represents the counter ion—anion like PF_6^-).[51]

terminates in a period shorter than 0.05 s. These results further demonstrate the storage energy mechanism of PEDOT is faradic redox reaction of doping/undoping, and the electrode reaction depth is controlled by reaction time. Therefore, the capacitance of the PEDOT electrode is mainly attributed to the pseudocapacitance originating from the fast doping/undoping process in spite that it has a low electric double-layer capacitance from the interface between electrolyte and active materials.

CONCLUSIONS

Porous PEDOT film electrodes without binder and conductive additive, successfully synthesized by an *in situ* chemical polymerization of microscale solution using ETA soft metal templates, have been used to construct supercapacitors with an organic electrolyte. Cyclic voltammetry and galvanostatic charging/discharging testing results show the good capacitive and rate performance of the PEDOT film electrodes. At the current density of ~0.2 A g^{-1}, the specific capacitance of the PEDOT supercapacitor is ~69.0 F g^{-1} or ~103.0 F m^{-2}, and the corresponding value of PEDOT electrode is 276.0 F g^{-1} and 206.0 F m^{-2}, respectively. The energy density decreases from ~24.0 to ~20.3 Wh kg^{-1} when the power density increases from ~420 to ~2080 W kg^{-1}. The columbic efficiency reaches above 95%, indicative of the good reaction reversibility of the PEDOT electrodes. The capacitance retention ratio was ~72% after 1500 charging/discharging cycles at the current density of 0.8 A g^{-1}, much higher than the reported polymers like PEDOT powders, PAN, PPy under the similar testing conditions. EIS curves are well fitted using the equivalent circuit model of $R_s(Q_l(R_i(Q_2R_f)(Q_3(R_{ct}W))))C_d$, and the analysis results further demonstrate the energy storage of PEDOT electrodes is mainly from fast Faradaic redox reaction in spite of a low electric double-layer capacitance. Furthermore, the PEDOT electrode reaction hardly takes place in a period shorter than 0.05 s.

The research results show that porous ETA templates can be used as both the microreactor for the solution polymerization and the current collector for the electrodes, which is different from conventional method to remove the templates after the formation of products. Symmetric flexible supercapacitors are readily constructed by sandwiching a microporous separator between two identical PEDOT electrodes. The PEDOT film on the porous surface of the ETA current collector are beneficial for the storage of electrolyte, the increase of accessible surface area and reaction active sites, the increase of the interface and close contact between active material and electrolyte, and the alleviation of volume change of active material during the charging/discharging process. Further improvement of the electrochemical performance of the obtained PEDOT film electrode by considering film thickness, polymerization conditions, conductive additive, redox material recombination, and post-treatment, is under investigation in our laboratory. It paves a simple and effective way to alleviate volume change of electrodes and prepare porous film electrodes without binders using soft metal templates for flexible electronic devices with good cyclic performance.

ACKNOWLEDGMENTS

We gratefully acknowledge the financial support from the National Science Foundation of China (Grant No. 21206099).

REFERENCES

1. Rogers, J. A.; Huang, Y. *Proc. Natl. Acad. Sci.* **2009**, *106*, 10875.
2. Béguin, F.; Szostak, K.; Lota, G.; Frackowiak, E. *Adv. Energ. Mater.* **2005**, *17*, 2384.
3. Zhou, G.; Li, F.; Cheng, H.-M. *Energ. Environ. Sci.* **2014**, *7*, 1307.
4. Shi, S.; Xu, C.; Yang, C.; Li, J.; Du, H.; Li, B.; Kang, F. *Particuology* **2013**, *11*, 371.
5. Conway, B. E. Electrochemical Supercapacitors: Scientific Fundamentals and Technological Applications; Kluwer Academic/Plenum Publishers: New York, **1999**.
6. Lv, P.; Feng, Y. Y.; Li, Y.; Feng, W. *J. Power Sources* **2012**, *220*, 160.
7. Wang, G.; Zhang, B.; Yu, Z.; Qu, M. *Solid State Ionics* **2005**, *176*, 1169.
8. Xing, W.; Li, F.; Yan, Z.-F.; Lu, G. Q. *J. Power Sources* **2004**, *134*, 324.
9. Hu, X.; Huai, Y.; Lin, Z.; Suo, J.; Deng, Z. *J. Electrochem. Soc.* **2007**, *154*, A1026.
10. Wang, Y.; Xia, Y. *Electrochem. Commun.* **2005**, *7*, 1138.
11. Wang, G.; Qu, M.; Yu, Z.; Yuan, R. *Mater. Chem. Phys.* **2007**, *105*, 169.
12. Amatucci, G. G.; Badway, F.; Du Pasquier, A.; Zheng, T. *J. Electrochem. Soc.* **2001**, *148*, A930.
13. Ryu, K. S.; Lee, Y.-G.; Hong, Y.-S.; Park, Y. J.; Wu, X.; Kim, K. M.; Kang, M. G.; Park, N.-G.; Chang, S. H. *Electrochim. Acta* **2004**, *50*, 843.

14. Österholm, A. M.; Shen, D. E.; Dyer, A. L.; Reynolds, J. R. *ACS Appl. Mater. Interfaces* **2013**, *5*, 13432.
15. Patra, S.; Munichandraiah, N. *J. Appl. Polym. Sci.* **2007**, *106*, 1160.
16. Ran, L.; Seung Il, C.; Sang Bok, L. *Nanotechnology* **2008**, *19*, 215710.
17. Muthulakshmi, B.; Kalpana, D.; Pitchumani, S.; Renganathan, N. G. *J. Power Sources* **2006**, *158*, 1533.
18. Ammam, M.; Fransaer, J. *Chem. Commun.* **2012**, *48*, 2036.
19. Chen, T.; Dai, L. *J. Mater. Chem. A* **2014**, *2*, 10756.
20. Sangermano, M.; Chiolerio, A.; Veronese, G. P.; Ortolani, L.; Rizzoli, R.; Mancarella, F.; Morandi, V. *Macromol. Rapid. Comm.* **2014**, *35*, 355.
21. Sangermano, M.; Vitale, A.; Razza, N.; Favetto, A.; Paleari, M.; Ariano, P. *Polymer* **2015**, *56*, 131.
22. Chi, H. Z.; Tian, S.; Hu, X.; Qin, H.; Xi, J. *J. Alloy. Compd.* **2014**, *587*, 354.
23. Yang, W.; Gao, Z.; Ma, J.; Zhang, X.; Wang, J.; Liu, J. *J. Mater. Chem. A* **2014**, *2*, 1448.
24. Kim, B. C.; Too, C. O.; Kwon, J. S.; Ko, J. M.; Wallace, G. G. *Synthetic. Met.* **2011**, *161*, 1130.
25. Mastragostino, M.; Arbizzani, C.; Soavi, F. *J. Power Sources* **2001**, *97–98*, 815.
26. Spinks, G. M.; Wallace, G. G.; Carter, C. D.; Zhou, D.; Fifield, L. S.; Kincaid, C. R.; Baughman, R. H. *Smart Str. Mater. Electroactive Polym. Actuators Devices* **2001**, *4329*, 199.
27. Zhao, Q.; Sun, Y.; Wang, G.; Wu, W.; Luo, C.; Yan, K.; Lu, H. *Synth. Met.* **2013**, *163*, 42.
28. Döbbelin, M.; Tena-Zaera, R.; Carrasco, P. M.; Sarasua, J. R.; Cabañero, G.; Mecerreyes, D. *J. Polym. Sci. A: Polym. Chem.* **2010**, *48*, 4648.
29. Mao, H.; Lu, X.; Liu, X.; Tang, J.; Wang, C.; Zhang, W. *J. Phys. Chem. C* **2009**, *113*, 9472.
30. Kim, M.; Yoo, J.; Im, H.; Kim, J. *J. Power Sources* **2013**, *230*, 1.
31. Wang, G.; Shao, Z.; Yu, Z. *Nanotechnology* **2007**, *18*, 205705.
32. Laforgue, A.; Robitaille, L. *Macromolecules* **2010**, *43*, 4194.
33. Laporta, M.; Pegoraro, M.; Zanderighi, L. *Phys. Chem. Chem. Phys.* **1999**, *1*, 4619.
34. Guixin, W.; Zongping, S.; Zuolong, Y. *Nanotechnology* **2007**, *18*, 6.
35. Selvakumar, M.; Krishna Bhat, D. *J. Appl. Polym. Sci.* **2008**, *107*, 2165.
36. Sahoo, S.; Dhibar, S.; Hatui, G.; Bhattacharya, P.; Das, C. K. *Polymer* **2013**, *54*, 1033.
37. Subramania, A.; Devi, S. L. *Polym. Adv. Technol.* **2008**, *19*, 727.
38. Gireaud, L.; Grugeon, S.; Pilard, S.; Guenot, P.; Tarascon, J. M.; Laruelle, S. *Anal. Chem.* **2006**, *78*, 3688.
39. Kang, H.; Wang, G.; Guo, H.; Chen, M.; Luo, C.; Yan, K. *Ind. Eng. Chem. Res.* **2012**, *51*, 7923.
40. Rui, X. H.; Ding, N.; Liu, J.; Li, C.; Chen, C. H. *Electrochim. Acta* **2010**, *55*, 2390.
41. Macdonald, J. R. *Ann. Biomed. Eng.* **1992**, *20*, 289.
42. Bobacka, J.; Lewenstam, A.; Ivaska, A. *J. Electroanal. Chem.* **2000**, *489*, 17.
43. Asplund, M.; von Holst, H.; Inganäs, O. *Biointerphases* **2008**, *3*, 83.
44. Carlberg, J. C. *J. Electrochem. Soc.* **1997**, *144*, L61.